Article:
Yao, G orcid.org/0000-0002-3292-2152, Zhao, J, Shen, X et al. (2 more authors) (2020) Effects of rheological properties on heat transfer enhancements by elastic instability in von-Karman swirling flow. International Journal of Heat and Mass Transfer, 152. 119535. p. 119535. ISSN 0017-9310

https://doi.org/10.1016/j.ijheatmasstransfer.2020.119535

Effects of Rheological Properties on Heat Transfer Enhancements by Elastic Instability in von-Karman Swirling Flow

Guice Yao[1, 2], Jin Zhao[3], Xiaobin Shen[2], Haie Yang[2], Dongsheng Wen[1, 2, 3*]

[1]School of Chemical and Process Engineering, University of Leeds, Leeds, LS2 9JT, United Kingdom

[2]School of Aeronautic Science and Engineering, Beihang University, 100191, Beijing, P.R. China

[3]School of General Engineering, Beihang University, 100191, Beijing, P.R.China

d.wen@leeds.ac.uk & d.wen@buaa.edu.cn

ABSTRACT

Elastic instability is proposed as a promising method to intensify heat transfer under very low Reynolds number conditions. However, the onset of elastic instability and its influence on heat transfer is highly dependent on the rheological properties of polymer solution, which has not been revealed. By varying polymer concentration, sucrose proportion and the degree of salinity, the heat transfer performance due to the variations of rheology is investigated in a swirling flow configuration between parallel plates. The results indicate that both the increase of polymer concentration and the reduction of the salinity can induce elastic instability easily, leading to a better heat transfer performance when the swirling velocity is fixed. However, the salinity effects become weakened as the swirling velocity continually increases and the maximum enhancement seems to be independent on salinity. In particular, the heat transfer performance based on pure elastic instability shows larger enhancement than that of inertial-elastic instability at low Reynolds number.

Keywords: Elastic turbulence; elastic instability; polymer; Swirling flow; rheology; heat transfer

1. Introduction

Efficient heat transfer plays an important role in many industrial sectors including power generation, information computing technology, chemical production, and ultra-high heat flux encountered in aerospace field [1]. Driven by industrial needs of process intensification and device miniaturization, the development of high-performance heat transfer technique at low Reynolds number, *Re*, has been intensively investigated in the past a few decades [2]. A conventional method to intensify heat transfer at low Re number is to induce turbulent-like flow motion by geometrical modifications [3-7], which however is not always practical due to the laminar flow nature encountered.

One of the proposed approaches is to use viscoelastic fluid, which is usually formed by adding small amounts of high-molecular-weight polymer into a pure Newtonian solvent [8]. This viscoelastic fluid exhibits dramatic flow instability in the presence of elastic nonlinearity, which is characterized by a normalized Weissenberg number, defined as $Wi=\dot{\gamma}\cdot\lambda$, where $\dot{\gamma}$ is the shear rate applied to the flow and λ is the polymer relaxation time. In particular, when the inertial effect is neglected at vanishing Reynolds number, the viscoelastic fluid is pronounced to induce purely elastic instability at $Wi > 1$ [9-11], and with further increase of the value of *Wi*, the flow is excited to a so called elastic turbulence regime [12, 13].

The occurrence of elastic instability or turbulence is attributed to the coupling effects between the stretch of long polymer chains induced by the shear stress and counteractive perturbations to the primary flow [14]. This turbulent-like phenomenon has been identified in many conventional geometries both in macroscale and microscale, including swirling flow between two parallel plates [15-17], Taylor-Couette flow set-up [18-20], curvilinear serpentine channel [18, 21-23] and some self-designed geometries such as cross slot channel [24, 25] and straight channel with obstacles inserted [26, 27]. Although whether the curvature of the flow geometry is an essential condition for the onset of elastic instability is still controversial, the transition to the elastic turbulence is always accompanied by a sharp growth of the flow resistance, which is similar to the features of inertial turbulence. In addition, the elastic turbulence has been proved to be an effective method to intensify the mixing performance [28-30].

It would be expected that such vigorous mass transport and dramatic increase in the flow resistance could affect the heat transfer, which however has received little attention [31]. Traore et al [32] investigated the effective heat conduction in a bulk fluid by a sucrose-based polymer solution in a swirling flow between parallel disks, where heat was transferred four time rapidly than that in a pure sucrose solution. Besides, a convective heat transfer performance up to 380 % between the fluid and the wall was achieved in a millimetre-sized curvilinear channels by Abed et al [33, 34]. An enhancement up to two orders of magnitude higher was observed by using polymer aqueous solution without sucrose as the size of the curvilinear channel was scaled down to micro meter size by Li et al [35, 36]. A few other experiments [37-42] were conducted in different geometries, and all showed the capability of elastic turbulence in improving heat transfer performance with the presence of different levels of heat transfer intensification.

It shall be noted that our current understanding on elastic turbulence and its relationship with heat transfer are still highly limited. The enhancement of heat transfer begins after the occurrence of elastic instability, which is highly dependent on polymer rheology [9-11]. However, few studies were focused on this area and only rheology effects based on polymer concentration were investigated. Even within these published studies there are still some inconsistent results. For example, the heat transfer enhancement against *Wi* increases with increasing polymer concentration in Refs [34, 43], which contradicts to the observation of Li et al [36]. Indeed, polymer rheology being sensitive with many other factors that could affect the heat transfer performance has not received attention so far [34, 44]. It becomes clear that the variations of polymer concentration and solvent viscosity could modify polymer rheological and elastic property significantly, whose effects on the heat transfer side, however, have not considered. Specially, with functional groups modification, the polymer rheology is affected by many water chemistry elements. The hydrolysed polyacrylamide (HPAM), which is capable of inducing elastic turbulence in porous media for enhancing oil recovery (EOR) [45-47], is sensitive to the surrounding ion effects due to the charged carboxylate groups [48]. The presence of different ions, typified by the salinity effect, is prevail in most of oil reservoirs and shall have large impacts on the polymer rheological properties [49], whose effects on the heat transfer have not been investigated as well.

Addressing these limitations, this work aims to conduct a systematic study to reveal the effects of polymer rheological properties on the heat transfer performance by elastic turbulence in a swirling flow configuration between two parallel plates. The rheological properties, including viscosity and polymer relaxation time, based on various polymer concentration, sucrose concentration and salinity are first evaluated. By mounting thermocouples along the gaps between the two plates, the corresponding temperature distribution are measured. To quantitatively characterize the concomitant heat transfer performance, both effective thermal conductivity and surface heat transfer Nusselt number are defined to characterize the heat transfer augments within bulk fluid and between the fluid and wall, respectively.

2. Materials and methods

2.1 Experimental system (set-up)

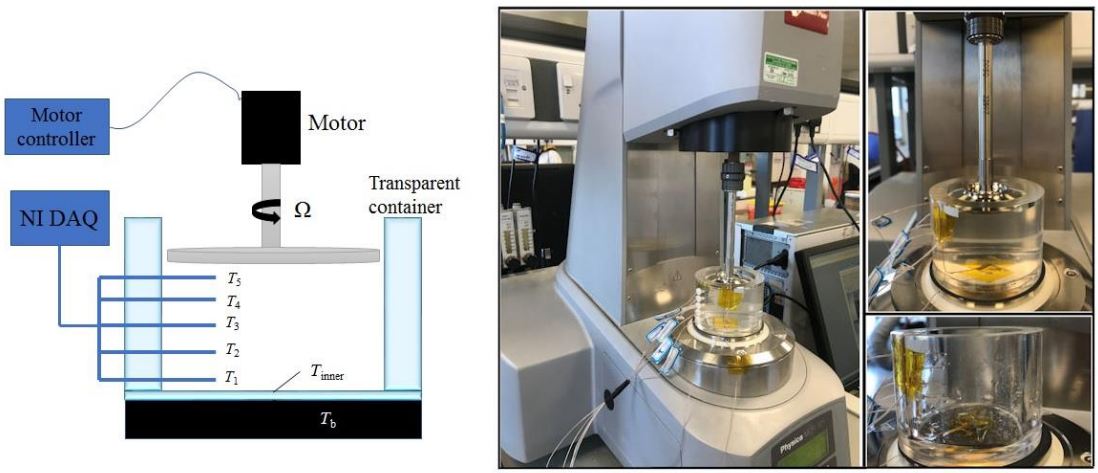

Fig. 1 Schematic view of the experimental setup

The experimental rig used to investigate the behaviour of the flow and convectional heat transfer performance of viscoelastic fluids in swirling flow is shown in Fig. 1. It consists of an acrylic fluid container with the inner diameter of D_{in}=56 mm and surrounded by optically transparent walls. The thicknesses of side wall and bottom wall are 10 mm and 5 mm, respectively. The flow is driven by a rotating round disk with a radius R_d=25 mm mounted on the shaft of the rheometer. The distance between the top disk and the inner wall of the bottom of the fluid container is set at a constant value, H=40 mm, for all experiments. The bottom of the fluid container is mounted at the base of the rheometer and the temperature of which is set to a value of 5 °C during experiments to reduce thermal convection inside the bulk flow. To ensure a good

repeatability and reproducibility of the experiments, the room temperature was maintained around 22 °C by an air conditioning system.

Two thermocouples were mounted on both sides of the bottom of the fluid container to measure the temperatures and to calculate the heat flux transferred between bulk fluid and the wall. The temperature distribution of the flow is monitored by an array of five thermocouples (T_1 to T_5) installed equidistantly (5mm each point) along the vertical direction z and positioned at the radial position at half radius of the fluid container. All thermocouples used in this work are K-type thermocouples with probe diameter of 0.25 mm and are calibrated against a mercury thermometer of certified accuracy (± 0.3 °C) in ice water mixture. The signals of the thermocouples are collected by national instrument data acquisition system (NI 9185) and post-analysed by LabVIEW software.

2.2 Working fluids preparation

The working fluids applied in this study were comprised of different amounts of hydrolysed polyacrylamide (HPAM), sucrose and sodium chloride (NaCl). Sucrose and sodium chloride with laboratory reagent grade were supplied by Fisher Scientific Ltd. The HPAM with molecular weight 22M g/mole were purchased from Shandong Tongli Chemical Co., Ltd. (China). A concentrated HPAM solution with 2000 ppm was prepared first. By adding specific amounts of concentrated HPAM solution, sucrose and NaCl into deionized water, the working fluids were then well prepared after 3h moderate mixing by a mechanical stirrer and stayed overnight to degrade the polymer with the largest molecular weight. With each variable was set different, the effects of polymer concentration, solvent viscosity and degree of salinity were investigated, respectively. The overview of working fluids is listed in the Table 1. To reduce the effects of polymer molecular weight and the long-time instability, the working fluids of experiments for each sensitive factor were freshly prepared with the same concentrated stock solution before the measurement to obtain a good repeatability.

Table 1 Working fluids applied in this study

Controlled parameters	Index	HPAM (ppm)	Sucrose (%)	NaCl (%)	Thermal conductivity ($W \cdot m^{-1} \cdot K^{-1}$)
Polymer concentration	1	100	65	1	0.356
	2	200	65	1	0.372
	3	300	65	1	0.366
Degree of salinity	1	200	65	0	0.362

	2	200	65	0.1	0.364
	3	200	65	0.5	0.373
Proportion of solvent	1	200	0	1	0.563
	2	200	20	1	0.510
	3	200	40	1	0.453
	4	200	65	1	0.362

2.3 Data analysis method

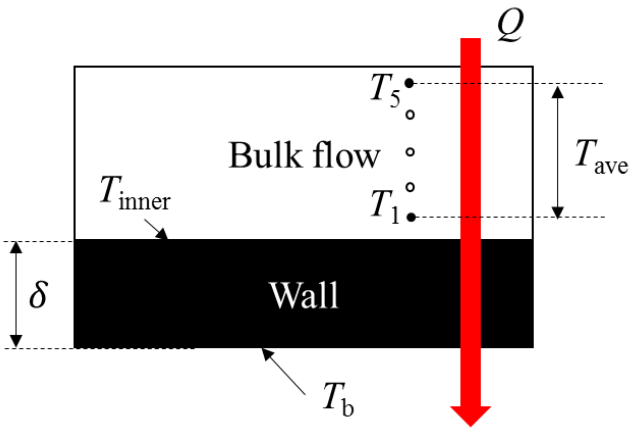

Fig. 2 Schematic diagram of the heat transfer process during experiments

The heat transfer process is schematically drawn in Fig. 2. The amount of heat flux removed by the cooling plate can be quantitatively calculated by equation (1).

$$Q = k_{acrylic} \cdot \frac{T_{inner} - T_b}{\delta} \tag{1}$$

where δ is the thickness of the acrylic wall, T_{inner} and T_b are the temperatures of the top and the bottom surface of the wall, respectively; $k_{acrylic} = 0.18\ W \cdot m^{-1} \cdot K^{-1}$ is the standard thermal conductivity of acrylic materials. To evaluate the heat transfer performance, the effective thermal conductivity, k^*, and the global heat transfer coefficient, h^*, are adopted here to characterize the heat transfer enhancement inside the bulk fluid and between the fluid and the wall, which are represented by equations (2) and (3), respectively:

$$k^* = \frac{Q}{\frac{T_5 - T_1}{x_5 - x_1}} \cdot \tag{2}$$

$$h^* = \frac{Q}{(T_{ave} - T_{inner})} \tag{3}$$

where T_1 and T_5 are the equilibrated temperature of thermocouples mounted near the bottom and top plates, respectively; T_{ave} is the average temperature of working fluids and T_{inner} is the temperature of the bottom of the fluid container; x_1 and x_5 indicate the z-coordinates position of thermocouples T_1 and T_5. The corresponding Nusselt number can be obtained by equation (4).

$$Nu^* = \frac{h^* H}{k} \tag{4}$$

2.4 The uncertainties of experimental measurement

The uncertainties of the effective thermal conductivity and the averaged Nu come from the energy balance equation parameters [50]. The uncertainty of these experimental results are calculated as:

$$\varepsilon_{k^*} = \sqrt{\left\{\left(\frac{\varepsilon_{\Delta T_b}}{\Delta T_b}\right)^2 + \left(\frac{\varepsilon_\delta}{\delta}\right)^2 + \left(\frac{\varepsilon_{\Delta x}}{\Delta x}\right)^2 + \left(\frac{\varepsilon_{\Delta T_l}}{\Delta T_l}\right)^2\right\}} \tag{5}$$

$$\varepsilon_{Nu} = \sqrt{\left\{\left(\frac{\varepsilon_{\Delta T_b}}{\Delta T_b}\right)^2 + \left(\frac{\varepsilon_\delta}{\delta}\right)^2 + \left(\frac{\varepsilon_{\Delta H}}{\Delta H}\right)^2 + \left(\frac{\varepsilon_{\Delta k}}{\Delta k}\right)^2 + \left(\frac{\varepsilon_{\Delta T_m}}{\Delta T_m}\right)^2\right\}} \tag{6}$$

where, $\varepsilon_{k^*}$and ε_{Nu} are the percent uncertainty in calculating k^* and Nu. $\varepsilon_{\Delta Tb}$, $\varepsilon_{\Delta Tm}$, and $\varepsilon_{\Delta Tl}$, with value of ±0.3 °C, represent the uncertainty of the temperature differences between bottom walls, liquid and the inner wall, and bottom and top of the bulk liquid, respectively. ε_δ = ±0.1 mm is the uncertainty of the thickness of the bottom wall. $\varepsilon_{\Delta H}$ = ±0.1 mm is the uncertainty of the height between the upper plates and the inner wall of the bottom. $\varepsilon_{\Delta x}$ = ±0.1 mm is the uncertainty of the distance between the T_1 and T_5. $\varepsilon_{\Delta k}$ = ±2.4% represents the uncertainty of the measurement of thermal conductivities of the working fluids. The uncertainties for each experiment with different working conditions could be estimated by the equation (5) and (6). The minimum and maximum uncertainty values of k^* and Nu are demonstrated in Table 2 for all working fluids, while the others are displayed as error bars in the figures shown in the following sections. It should be noted that the most uncertainty in determining Nu came from the measured temperatures of the walls and fluids, approximately over 90% of the total error, whilst the others such as the determination of the thermal conductivity and the gap between the two plates contribute the remaining error.

As shown in the later, the agreement between the averaged Nu from the experimental results and the simulation for the pure sucrose solution suggests the estimated uncertainties are reasonable. In addition, two repetitive experiments were conducted for

the pure sucrose solution and the HPAM solution with 65% sucrose and 1% NaCl. Both repetitions show similar trends with previous experiments and the measured *Nu* values are within the error tolerance.

2.5 Rheology investigation

The rheological properties of working fluids were measured by a cone and plate geometry in a stress-controlled rheometer (Anton Paar MCR 301) at a temperature of 15 °C, which is similar with the average temperature of bulk fluid. The effects of polymer concentration on the rheology are shown in Fig. 3. The viscosity increases with increasing polymer concentration for a given shear rate, which is ascribed to the increased frictional effects among polymer chains. All curves exhibit a shear-thinning behaviour whereas a higher polymer concentration induces more dramatic reduction. Fig. 3(b) shows the response of complex viscosity profiles as a function of angular velocity for different polymer concentrations. The results show both the out-of-phase viscosity and in-phase viscosity increase as the polymer concentration increases. The values for polymer-driven in-phase and out-of-phase viscosity were obtained by excluding the solvent contribution at same working conditions, $\eta_p' = \eta' - \eta_s'$ and $\eta_p'' = \eta'' - \eta_s''$, respectively. Then the polymer relaxation time was calculated according to equation (7), as shown in Fig. 3(c) for the 200 ppm HPAM solution with 65% sucrose and 1% NaCl at different shear rates. The dependence of the polymer relaxation time on the shear rate with different polymer concentration is shown in Fig. 3(d). Both curves show a clear shear thinning behaviour as a function of the shear rate, with scaling $\lambda \sim \dot{\gamma}^{-\alpha}$, similar to previous investigation in Ref [51], which also explains why the increase of *Wi* is normally slower than the increase of shear rate. In addition, with higher polymer concentration, the polymer relaxation time becomes longer, leading to an increased elasticity of HPAM solution, which may contribute to the onset of elastic turbulence or instability.

$$\lambda = \lim_{\omega \to 0} \left\{ \frac{1}{\omega} \left[\frac{\eta_P''(\omega)}{\eta_P'(\omega)} \right] \right\} \tag{7}$$

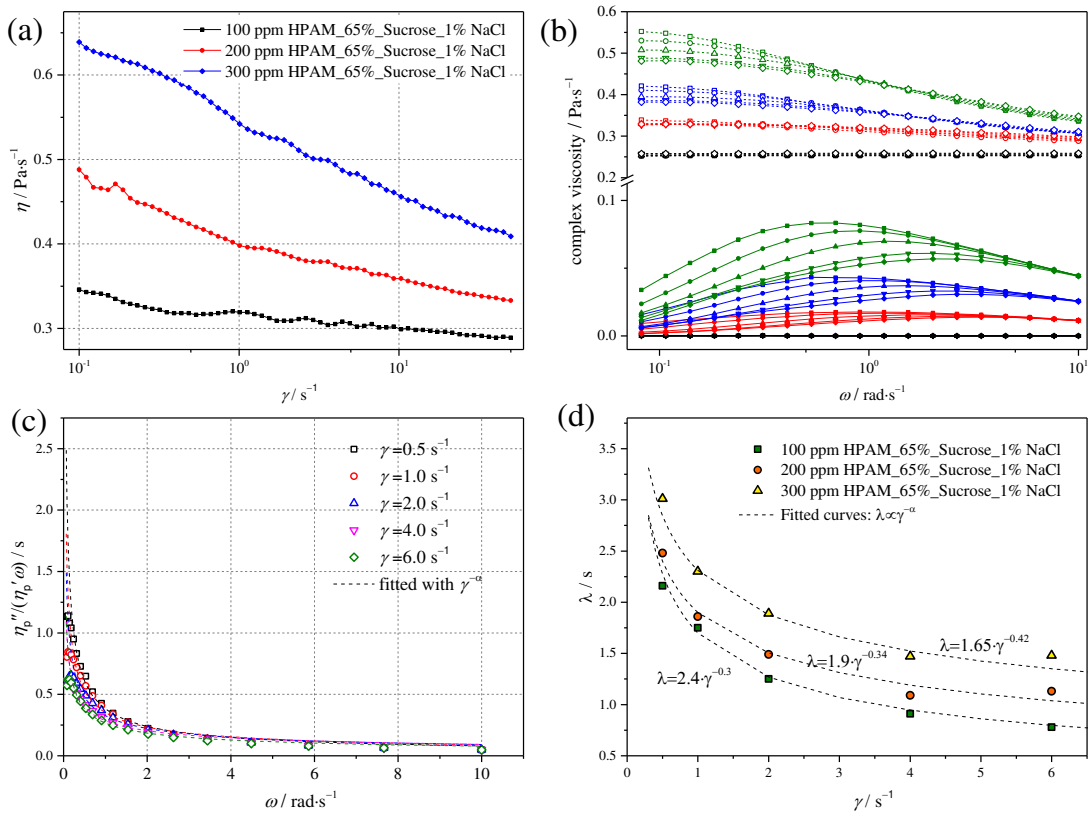

Fig. 3 The variations of polymer rheology with polymer concentration. (a) The viscosity profiles as a function of shear rate with different polymer concentration; (b) The measured complex viscosity at oscillating mode with different shear rate; (c) Angular frequency dependence of $\eta_p''/(\eta_p'\omega)$ for 200 ppm polymer solution, (d) The shear rate dependence of polymer relaxation time with different polymer concentration

Fig. 4 highlights the salinity effects on the rheology of polymer solution. The presence of salts has a buffering effect, shielding the charges along the polymer chain with salt cations, resulting in polymer molecules shrinkage and consequent viscosity reduction. This shrinkage also contributes to the alignment of polymer molecules, which significantly reduces the shear-thinning phenomenon. As the shielding effect is limited by the numbers of charge groups along the polymer chain, a critical salinity value shall exist, above which the salinity effect become ineffective. With continuous increase of the salinity, a so-called poor solvent is obtained, i.e., increasing the polymer interactions would lead to an increase of viscosity. In such conditions, the salinity is not the only influential parameter anymore. In this study, the salinity of 1% was excluded to eliminate the effects of poor solvent. The corresponding relaxation times with different salinity are concluded in Fig. 4(d).

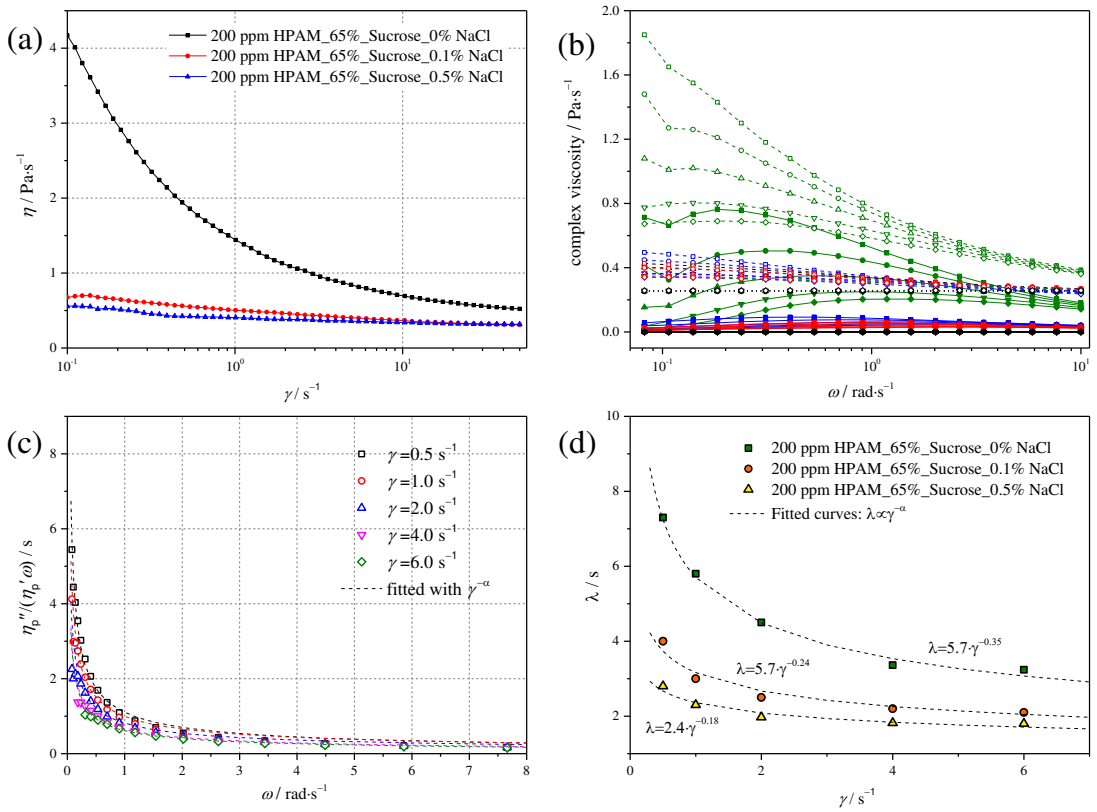

Fig. 4 The variations of polymer rheology with salinity. (a) The viscosity profiles as a function of shear rate with different salinity; (b) The measured complex viscosity at oscillating mode with different shear rate; (c) Angular frequency dependence of $\eta_p''/(\eta_p'\omega)$ for 200 ppm polymer solution with 0% NaCl, (d) The shear rate dependence of polymer relaxation time with different salinity

Fig. 5 demonstrates the effects of solvent on the rheological properties of polymer solutions by varying the proportion of sucrose. With the addition of sucrose into the polymer solution, as expected, both the viscosity and relaxation time increase, which is consistent well with previous investigations that the polymer relaxation time is proportional to the viscosity of solvent [11]. One can see that the difference between polymer solution with 20% sucrose and 40% sucrose is small, which interprets why at high applied swirling velocity, the heat transfer enhancement of polymer solution with 20% sucrose is better than that of 40% sucrose.

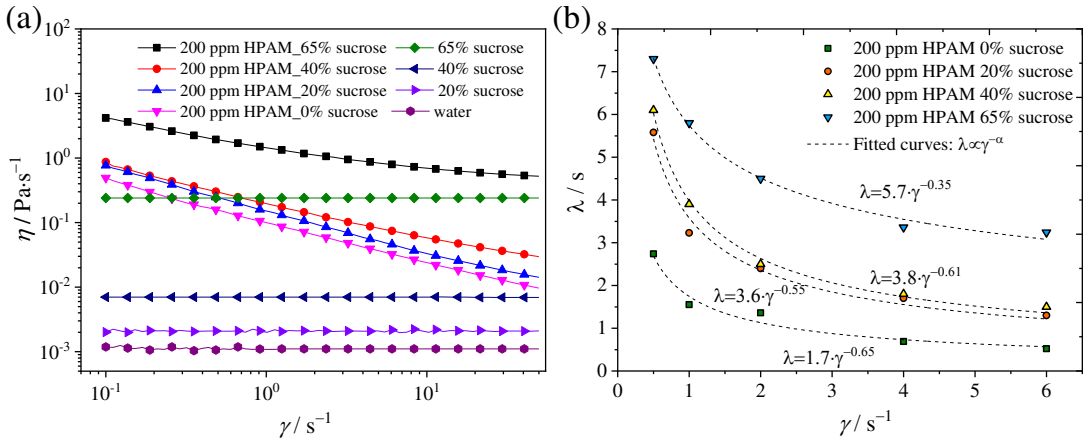

Fig. 5 Effects of sucrose proportion on the rheology of polymer solution. (a) Viscosity profiles of working fluids applied in the following investigation; (b) Shear rate dependence on polymer relaxation time for polymer solution with different amount of sucrose addition

3. Results and Discussions

The heat transfer behaviours of all working fluids were conducted at rotating speed ranging from 0 to 14 rpm. It should be noted that the shear rate within the bulk fluids was highly inhomogeneous due to the large gaps between the two parallel plates. The shear rate hence was modified based on the viscosity profiles for pure sucrose solutions, as shown in Fig. S1 in the supplementary document. A normalised reduced temperature θ, calculated as equation (8), was applied to represent the temperature profiles along the axial direction.

$$\theta = \frac{T_0 - T}{T_0 - T_b} \tag{8}$$

3.1 Effects of polymer concentration

The equilibrated reduced temperatures along the vertical direction as a function of rotating speed with different polymer concentration are shown in Fig. 6. Without rotation, the temperature distribution along the vertical direction are in layers and the temperature difference between neighbouring thermocouples are almost similar. With the top disk starting to rotate, for polymer solutions, the temperature distribution gradually tends to be homogeneous as the speed increases, which indicates the existence of irregular flows. In comparison with pure sucrose solution, such flow instability is attributed to the elastic stress rather than viscous stress due to there is no collapsing phenomenon observed in the latter case. The interaction between polymer coil-stretch transition and the primary flow induces the secondary flow along the vertical direction, which accelerates the heat transfer and unifies the temperature. Especially, when the

polymer concentration is higher, more numbers of polymer reacts with the primary flow. Therefore, at same rotation, the concentrated polymer solution intends to generate more intensive elastic flow instability, which strengthens the temperature homogeneity in the bulk.

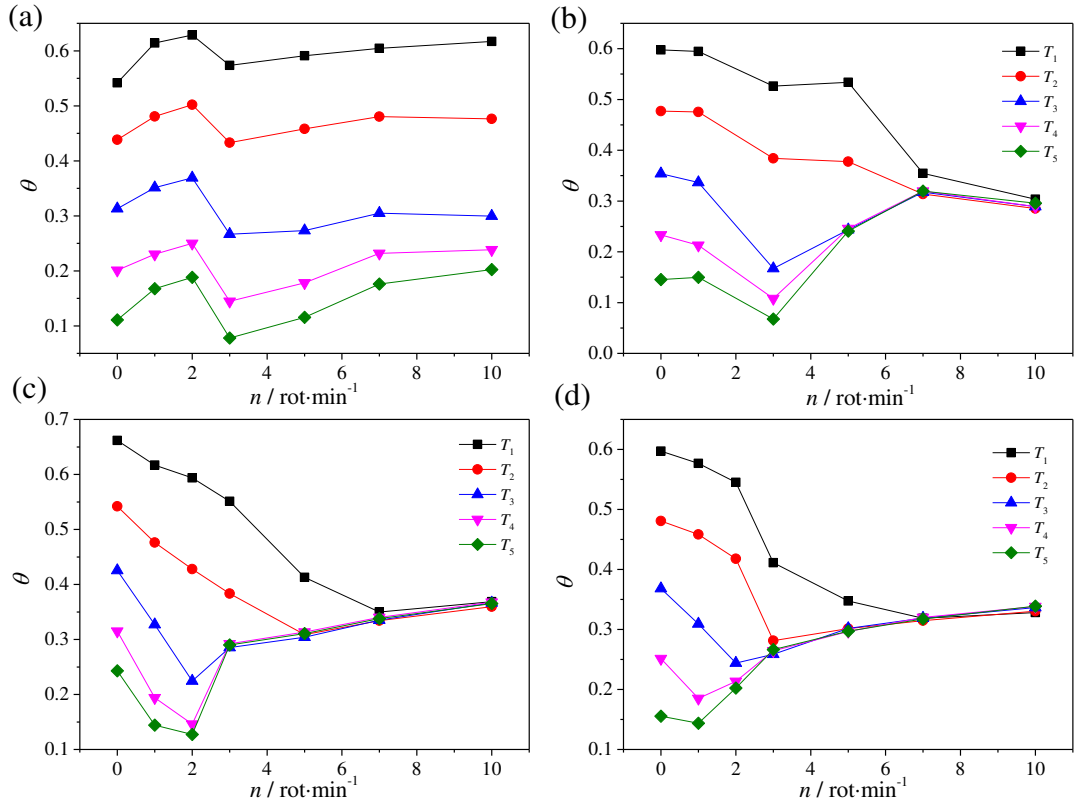

Fig. 6 Equilibrated reduced temperature profiles of pure sucrose solution and polymer solutions with different concentration: (a) pure 65% sucrose solution with 1% NaCl, (b) 100 ppm HPAM sucrose solution with 65 % sucrose and 1% NaCl, (c) 200 ppm HPAM sucrose solution with 65 % sucrose and 1% NaCl, (d) 300 ppm HPAM sucrose solution with 65 % sucrose and 1 % NaCl

To quantitatively evaluate the onset of elastic instability and the heat transfer augment due to elastic instability, the effective thermal conductivity and the convective Nusselt number are shown in Fig. 7 and Fig. 9. The effective thermal conductivity represents the heat conduction within the bulk. A sharp increase of that could be regarded as a signal of the onset of elastic instability. It is clear found that polymer solution with higher concentration is much easily to induce elastic instability as demonstrated in Fig. 7(a). The critical rotating speed to induce elastic instability is estimated varying from 4.2 rpm to 1 rpm when the polymer concentration increases from 100 ppm to 300 ppm, respectively. The corresponding critical Wi_c numbers is also reduced, which is consistent well the previous results in Ref [52]. Indeed, the elastic

instability is highly dependent on geometry gap ratio, d/R, polymer contribution to viscosity, η_p/η, and degree of stretching of the polymers by the base flow, Wi. With the shear thinning phenomenon is probably considered, the elastic instability threshold could be determined by a parameter K, defined as:

$$K \sim \frac{\eta_p}{\eta}\frac{d}{R}Wi^2 \tag{8}$$

The elastic instability then occurs when K exceeds a certain threshold. The polymer contribution to the viscosity is more significant with the increase of polymer concentration. Therefore, when the gap ratio is fixed, the Wi at the instability threshold should depend on it as $Wi_c \sim (\eta_p/\eta)^{-0.5}$, which results in the reduction of Wi_c. In the present work, the relationship between estimated Wi_c from the Fig. 7(b) and η_p/η from Fig. 3(a) is demonstrated in Fig. 8, where the dependence can be well fitted by the power law $Wi \sim (\eta_p/\eta)^{-\alpha}$, with the exponent $\alpha = 0.6$, which is quite close to the expected value of 0.5.

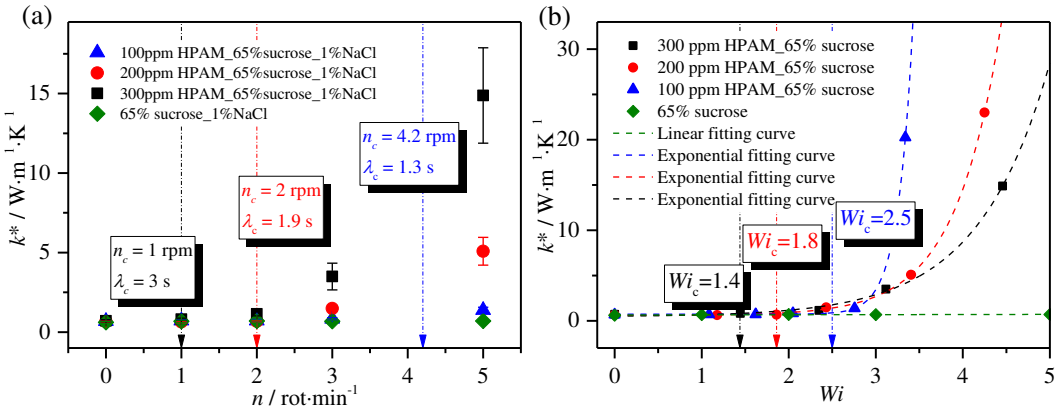

Fig. 7 The variations of effective thermal conductivity with different polymer concentrations (a) as a function of rotating speed and (b) as a function of Wi

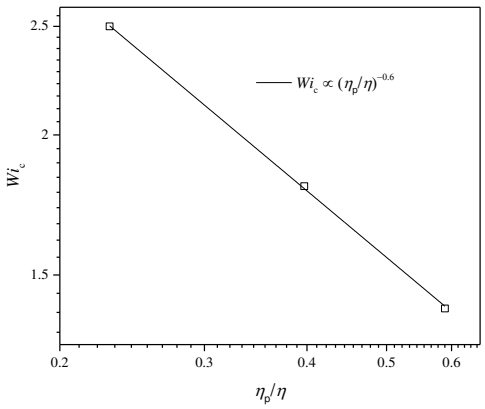

Fig. 8 The generalized Wi_c number as a function of η_p/η at the onset of elastic instability with different polymer concentrations

After the occurrence of elastic instability, a remarkable rise of k^* appears. For a given swirling flow, the polymer solution with higher concentration exhibits better heat transfer performance within the bulk, indicates that the degree of flow irregularity intensifies as the polymer concentration increases, which results in more heat is transferred between flow layers. The enhancement of effective thermal conductivity for the 300 ppm polymer solution could reach to 23 times larger than that of sucrose solution, which is even higher than the enhancement of inertial turbulence of a Newtonian fluid in swirling flow at Re=2500 [53], where 10 times incremental was obtained.

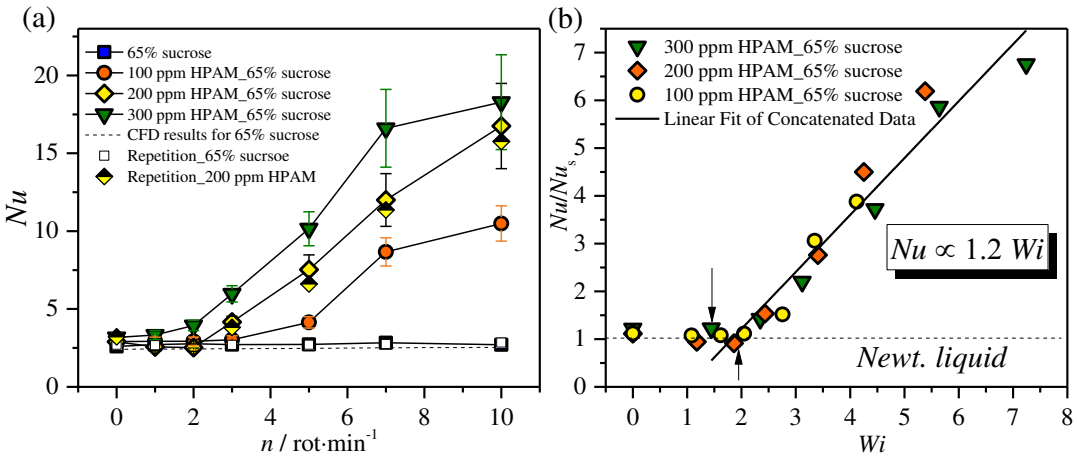

Fig. 9 The variations of convective heat transfer performance with different polymer concentration (a) as a function of rotating speed and (b) as a function of *Wi*

Fig. 9(a) demonstrates the *Nu* between wall and fluid against degree of rotation with different polymer solutions. Similar trends are observed with the results of effective thermal conductivity. The *Nu* increases with increasing the polymer concentration. When n=10 rpm, the convective heat transfer of 300 ppm HPAM solution can reach to 6 times more efficiency than that of the sucrose solution, which is in same orders with previous studies [32, 34, 37]. The small discrepancy is ascribed to the polymer properties and streamline curvature of the geometry. As discussed above, when the rotating speed is fixed, higher polymer concentration allows more polymer molecules to be stretched by the primary flow. Therefore, more elastic energies are diffused into flow kinetic energy, resulting in more dramatic turbulent behaviours, reducing the thermal boundary layer near the wall and transferring the heat more rapidly.

However, this dependence becomes different when the k^* and Nu are demonstrated as a function of Wi, where the polymer relaxation discrepancy is normalised. The polymer solutions with higher concentration still show slight heat transfer enhancement before the elastic instability is induced in lower concentration polymer solution. After the occurrence of the elastic instability, continually increase Wi, a steep enhancement in heat transfer is observed for all polymer solutions with the Nu collapsing linearly by $Nu \propto 1.2Wi$, which is consistent well with the observations from Ref.[34]. In dilute polymer solutions, due to the presence of the high salt concentrations, the shear thinning phenomenon is not such dramatic. Therefore, when the stretching degree of polymer solution (characterised by Wi) is in same level, the intensity of elastic instability should be similar, and the concomitant heat transfer enhancement shows similar behaviours. However, it should be mentioned that the saturation of fully developed elastic turbulence is limited by the polymer concentration. More numbers of polymer contribute to the stronger flow intensifications, which also implies that the experiments conducted here, the flow is still in transition regime and on its way to fully developed elastic turbulence.

3.2 Effects of salinity

In this section, the effects of salinity on the heat transfer performance are investigated. Fig. 10 describes the equilibrated reduced temperature distribution against rotating speed with different salinity. Increasing salinity makes the temperature distribution curves more difficult to converge. Especially, when the salinity is 0.5 %, even at the maximum applied rotating speed, the temperature distribution is still in layers, which indicates the flow haven't been fully perturbed. The salinity effect on the onset of elastic instability is estimated from the Fig. 11. The polymer solution with lower salinity is capable of inducing elastic instability at relatively smaller rotating velocity, n = 0.5 rpm, thereby perturbing the flow and intensifying the heat transfer within the bulk. While increasing the salinity, more driven forces and higher rotating velocity, n = 3.8 rpm are required to trigger the flow instability. As discussed above, with presence of salt cations, the polymer is shielded into a coiled state, leading to the reduction of the polymer relaxation time and viscosity. Therefore, the polymer solution with high salinity behaves more like Newtonian fluid and has less elasticity. In order to achieve the polymer coil-stretch transition, additional forces are required to overcome

the shielding effects and the occurrence of the elastic turbulence is postponed consequently.

The reduction of the salinity, on the other hand, induces significant shear-thinning phenomenon due to the realignment of the elongated polymer chains, which enlarges the polymer contributions to the viscosity. As a result, the critical Wi_c on the onset of elastic instability decreases. The dependence of estimated Wi_c from the Fig. 11 on the η_p/η is shown in the Fig. 12. The results can still be fitted with power law $Wi \sim (\eta_p/\eta)^{-\alpha}$. However, rather than expected value of 0.5, the exponent α goes higher to 0.95, which is consistent with our previous investigations [54]. The additional effects by shear-thinning which cannot be captured by the standard criterion of the onset of elastic instability were also investigated in curvilinear channel [34, 55]. The detailed mechanism of such effects is still missing. One possible interpretation is that there is an existence of second normal-stress difference may lead to a stabilizing effect of the flow. The magnitude of the second normal-stress difference is small compared to the first normal-stress difference (which is characterised by *Wi*) for weak shear thinning fluids. However, for strong shear-thinning fluids the second normal-stress difference may become important, and postpone the increase of the elastic instability, which as shown in Fig. 13, the *Nu* increases slowly with *Wi* for polymer solution with low salinity.

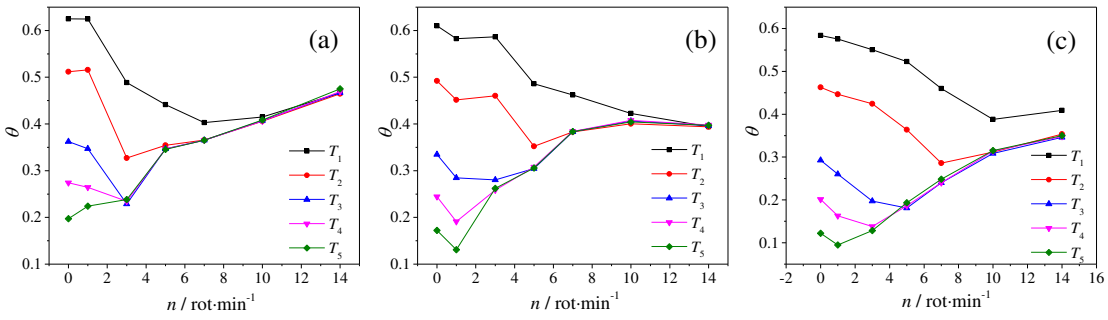

Fig. 10 Equilibrated reduced temperature profiles for polymer solutions with different salnity: (a) 200 ppm HPAM solution without salt; (b) 200 ppm HPAM solution with 0.1% NaCl; (c) 200 ppm HPAM solution with 0.5% NaCl

The effective thermal conductivity and convective Nusselt number with various salinity are displayed in Fig. 11 and Fig. 13, respectively. With same rotating velocity, the polymer solution with lower salinity exhibits better heat transfer performance which is mainly because the polymer relaxation time reduction by shielding effect decreases the elastic nonlinearity. However, this trend is different when the degree of the rotation exceeds a certain value, here n=10 rpm in this study. Similar *Nu* values which are

approximately 6 time higher than sucrose solution are obtained for all working fluids. Indeed, the total shear stress of the upper plate and the frequency power spectra of the flow velocity in the fully elastic turbulence regime are independent on salinity but limited by polymer concentration as shown in our previous study [54]. Therefore, the elastic flow irregularities on the primary flow are in similar level, which results in the analogous heat transfer augment. With such intensive flow irregularity, the motion of the salt ions and the polymer molecules is random and disordered, weakening the static electronic repulsion between each other, making the shielding effect insufficient Particularly, the *Nu* of the polymer solution with 0.5 % NaCl is smaller than that of other solutions with lower salinity, which is mainly because the elastic instability has not fully evaluated across the whole bulk fluid.

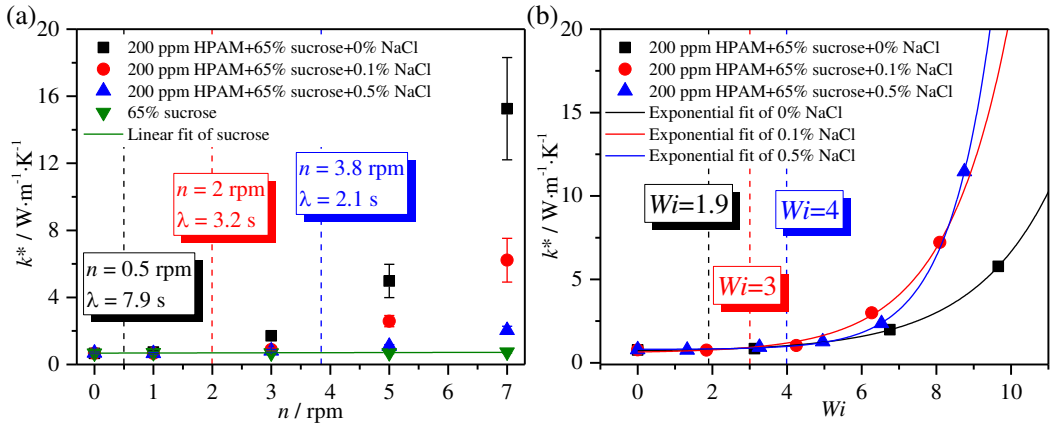

Fig. 11 Effects of degree of salinity on the effective thermal conductivity (a) as a function of rotating speed; (b) as a function of *Wi*

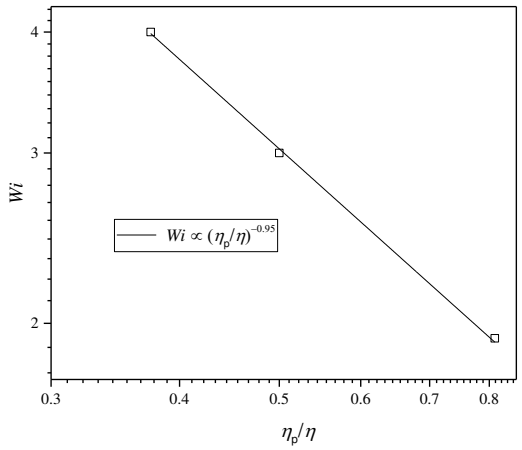

Fig. 12 The generalized Wi_c number as a function of η_p/η at the onset of elastic instability due to the existence of salt

It also should be noticed that the heat transfer enhancement after the occurrence of elastic instability for higher salinity seems to be more rapid, which also can imply

the insufficient effects of shielding effect at high swirling velocity. The onset of elastic instability is suppressed by the reduction of the polymer elasticity due to the shielding effect of cations. The more amounts of cations are, before the critical value based on the limitation of carboxylate groups are reached, the stronger the shielding forces are, and the more difficult for polymer solution to be perturbed. However, if the shielding effect is overcome by additional driven forces (increasing rotating speed), the elastic instability is induced, and the concomitant heat transfer performance increases. As discussed above, with increasing the flow velocity the shielding effect weakens, accelerating the flow irregularity and relative the heat transfer enhancement close to the polymer solution without salt.

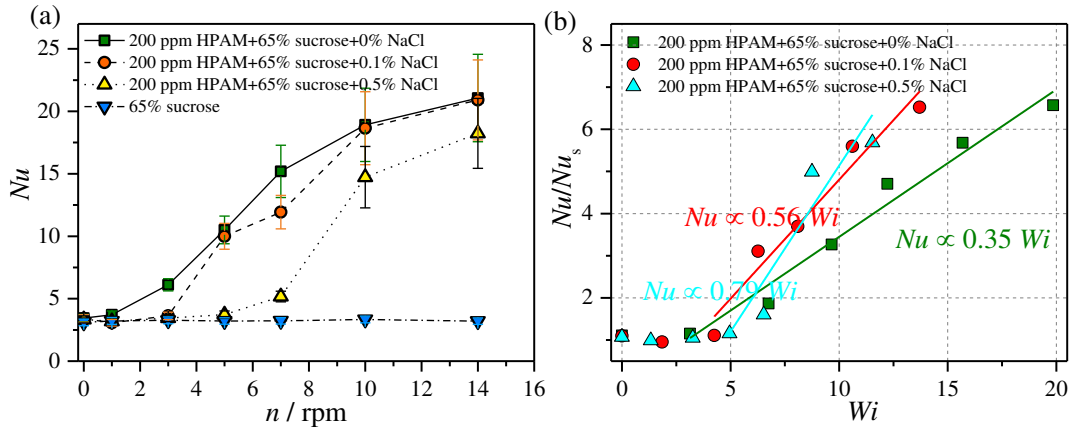

Fig. 13 Effects of degree of salinity on the convective heat transfer performance (a) as a function of rotating speed; (b) as a function of *Wi*

The salinity is not only reducing the polymer elasticity but also weaken the shear-thinning degree, which also has significant influences on the elastic instability or turbulence. By normalising the polymer elasticity, the variations of k^* and Nu^* as a function of *Wi* are presented in Fig. 11(b) and Fig. 13(b), respectively. Unlike the discussion for the effects of polymer concentration, the increase of *Nu* as a function of *Wi* is no longer concreated into a single curve but is highly dependent on the shear-thinning degree, indicating that the *Nu* is a function of both *Wi* and the degree of shear-thinning of the fluids. The significant shear-thinning phenomenon suppresses the evolution of *Nu*. As discussed above, for strong shear-thinning fluids, a stable secondary flow prevents the development of the flow instability, leading to the heat transfer enhancement increases slowly without expectation. Indeed, the shear rate inside the flow is more significant non-uniform of a strong shear-thinning fluid and these various gradients of shear force could balance with stretch of polymer to somehow,

which, as a result, the flow becomes stable and exhibits less heat transfer enhancement. The effects of shear thinning are quite complicated and further investigations are required to reveal the mechanism.

3 Effects of solvent concentration

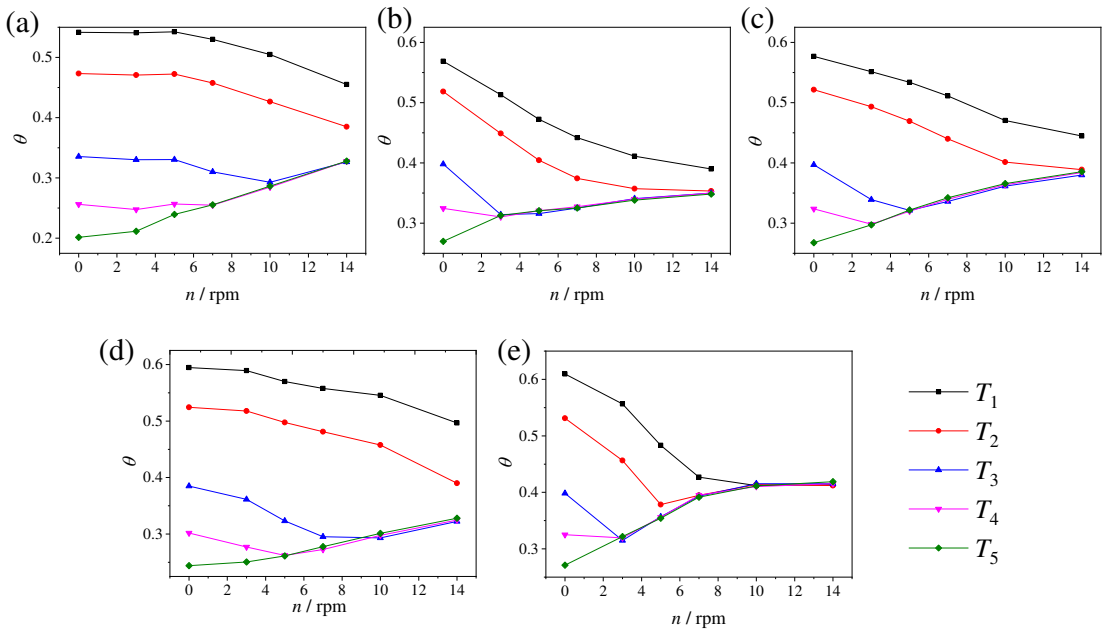

Fig. 14 Equilibrated reduced temperature profiles for polymer solutions with different amounts of sucrose addition: (a) pure water (b) 200 ppm HPAM solution without sucrose; (c) 200 ppm HPAM solution with 20% sucrose; (d) 200 ppm HPAM solution with 40% sucrose; (e) 200 ppm HPAM solution with 65% sucrose

The solvent effects were conducted in this section by varying the proportion of the sucrose of the polymer solution. The reduction of sucrose is expected to decrease the viscosity of the polymer solution as well as weaken the polymer relaxation capacity, which leads to a higher *Re* and a lower *Wi* at a given shear rate. On one hand, the increase of *Re* intensifies the inertial nonlinearity and makes the flow more instable. On the other hand, the highly reduction of the polymer relaxation time is less capable of inducing the elastic instability. The temperature distribution and the heat transfer performance for pure water were presented in Fig. 14 and 16, respectively. Compared with those of 65% sucrose solution, a clear increase of *Nu* is observed, which indicates the existence of the inertial instability. Therefore, by changing the proportion of sucrose from 65% to 0%, the flow instability is not solely driven by the elastic stress. A so called inertial-elastic instability should be considered instead. Based on the *Nu* profiles of water solution, the inertial nonlinearity could be neglected below n=7 rpm.

Besides the pure water solution, the reduced temperature distribution of polymer solutions with different sucrose concentrations are also shown in Fig.14. The temperature curves of polymer solutions without sucrose and with 65% sucrose additive are first collapsing, sequentially followed by polymer solutions with 20% sucrose and 40% sucrose, respectively, which indicates that the onset of flow instability is first postponed by increase the sucrose concentration and continually increasing will make the flow instability more easily induced. This could also be implied from the heat transfer performance in Fig. 16(b) at $n < 7$ rpm, where the flow instability is mainly ascribed to elastic instability. The instability criterion presented in equation (8) may not capture the effects of shear-thinning, however one can hope it still can serve least as a guide for a scaling relation in this case. The effects of addition of sucrose on the rheological properties of polymer solution is complicated. In the first place, the polymer contribution to the viscosity decreases with increasing the sucrose concentration as shown in Fig.15, which indicates a relatively smaller critical Wi_c is required to trigger the elastic instability. When the shear rate is fixed, the polymer solution with short polymer relaxation time can trigger the elastic instability. For another, the addition of sucrose enhances the polymer elasticity and concomitant polymer relaxation time becomes larger. Therefore, the occurrence of the elastic instability is determined by the combination of these two effects. When the sucrose concentration has not reach as high as 65 %, the polymer contribution to the viscosity is dominant, which makes the polymer solution with lower sucrose concentration is more easily to induce the elastic instability. However, when the sucrose concentration saturates at 65 %, the significant increase of the polymer relaxation time makes the polymer solution even at low shear rate can become instable. As a result, at low rotating speed of $n < 7$ rpm, the polymer solution with 65 sucrose shows best heat transfer performance, followed by 0%, 20% and 40%, respectively.

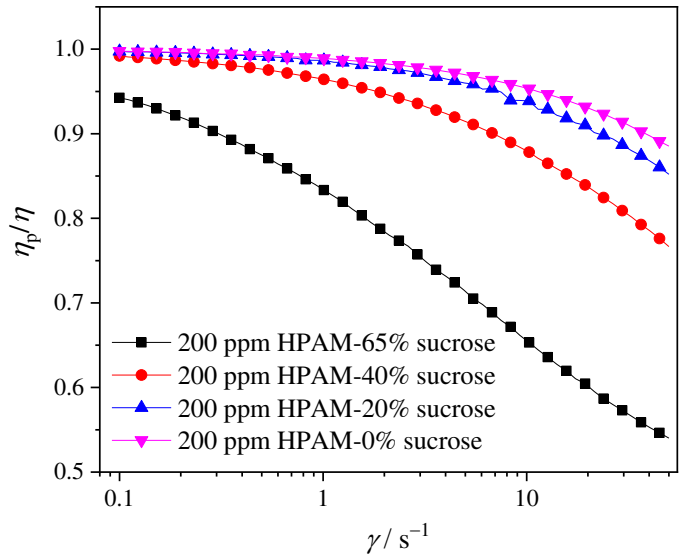

Fig. 15 The variations of polymer contribution to the viscosity with different sucrose addition

With increase of the rotating speed, the inertial instability exists after n > 7 rpm, where the heat transfer enhancement is not sole driven by the elastic instability and it should be influenced by the coupling effects between inertial and elastic nonlinearity. The heat transfer enhancement of the polymer solutions with 65 % sucrose is still most significant, followed by 20%, 0% and 40%, respectively. Compared with the pure HPAM solution, the HPAM solution with 20% sucrose can generate more intensively elastic irregularity due to the improvement of the polymer relaxation time, and the corresponding heat transfer performance increases. Continually increasing the sucrose concentration to 40%, the polymer elasticity does not change significantly, while the *Re* decreases rapidly which weakens the inertial instability and makes the heat transfer performance of the polymer solution with 40% sucrose even worse than pure HPAM solution without sucrose addition. Indeed, the elasticity numbers, *El*, of the polymer solutions with 20% and 40% sucrose are similar as shown in Fig. S4. The elasticity number represents the relative importance of elastic stress to inertial effect. With same *El*, the flow tends to small-scale vortex at high *Re* but large-scale at low *Re*. This small-scale vortex is much closer to the turbulent-like behaviours and results in a more significant enhancement of heat transfer [56]. When the sucrose concentration reaches to 65%, though the inertial nonlinearity does not exist anymore, the strong elastic nonlinearity perturbs the flow and enhance the heat transfer consequently. It also reveals that the heat transfer enhancement based on elastic instability at low flow rate is more dramatic than that based on inertial instability. Due to the low flow velocity,

the inertial instability is far from the turbulence region thereby the degree of flow irregularity is not strong enough. In other words, the elastic instability or elastic turbulence does a promising method for heat transfer intensification at low Re conditions.

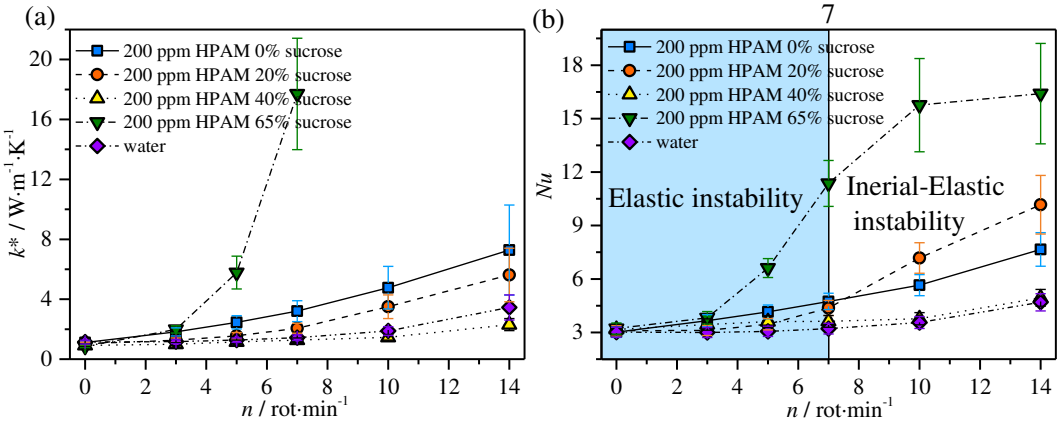

Fig. 16 Effects of sucrose concentration on (a) effective thermal conductivity; (b) Nusselt number as a function of rotating speed.

It is also should be noticed that the profiles of the effective thermal conductivity and convective *Nu* show different trends especially for polymer solutions with 0% and 20% sucrose. The effective thermal conductivity is dependent on the temperature distribution, which is highly sensitive with the onset of flow instability. It cannot reveal the amounts of heat removal from the wall, which is ascribed to the intensity of flow irregularity. Therefore, both the effective thermal conductivity and convective surface *Nu* are required to investigate the heat transfer performance within the bulk and between wall and liquid. In addition, the thermal conductivity of working fluids is different. The thermal conductivity decreases with increasing the sucrose concentration and such reduction declines the effective thermal conductivity as well. However, this discrepancy is delimited when calculates the *Nu* due to its definition.

4. Conclusions

Convective heat transfer performance under various polymer sensitive factors were investigated in a swirling flow configuration between two parallel disks. The bottom disk was cooled as a constant temperature of 5 °C with thermocouples mounted both on the wall and inside the flow, the Nu dependences on polymer concentration, solvent concentration and degree of salinity were achieved. The following conclusions can be obtained:

1. With the increase of the polymer concentration and reduction of the salinity, the onset of elastic instability shifts to an earlier critical swirling velocity and Weissenberg number. The heat transfer enhancement begins after the occurrence of elastic instability.
2. For a given swirling velocity, the enhancement increases with increasing polymer concentration. The maximum enhancement is dependent on polymer concentration. For a polymer solution with 300 ppm, the convective Nusselt number could reach more than 6 time higher than that of pure sucrose solution at the maximum rotating speed. After the occurrence of the elastic instability, the heat transfer enhancement exhibits linear relationship on Wi, i.e., $Nu/Nu_s \propto 1.2Wi$, which is independent on polymer concentration. This independence is attributed to the small discrepancies of shear-thinning in the dilute regime.
3. At low rotating speeds, the heat transfer enhancement increases with the reduction of the salinity for a giving swirling velocity. However, the enhancement becomes independent on the salinity when the swirling velocity exceeds a critical value, which is possible due to the reduction of the shielding effect. It becomes clear that the salinity influences the onset of elastic instability, but the maximum enhancement is limited by the polymer concentration. In addition, due to the significant discrepancies of shear-thinning, the Nu dependence on Wi varies with different salinities. The polymer solution with low salinity shows more dramatic shear-thinning phenomenon, suppressing the increase of the heat transfer enhancement.
4. The effects of solvent concentration on the enhancement is complicated due to the coupling effects between inertial and elastic nonlinearity. However, the enhancement based on pure elastic instability is the most dramatic and promising at low Reynolds numbers.

Acknowledgement

This work was supported by European Research Council through grant number 648375 and National Science Foundation of China Grant No. 51876006. The China Scholarship Council is appreciated for sponsoring the PhD study of G.Y.

Conflicts of interest

The authors declare no competing financial interest.

References

[1] M. Sheikholeslami, M. Gorji-Bandpy, D.D. Ganji, Review of heat transfer enhancement methods: Focus on passive methods using swirl flow devices, Renewable and Sustainable Energy Reviews, 49 (2015) 444-469.

[2] M. Sheikholeslami, B. Rezaeianjouybari, M. Darzi, A. Shafee, Z. Li, T.K. Nguyen, Application of nano-refrigerant for boiling heat transfer enhancement employing an experimental study, International Journal of Heat and Mass Transfer, 141 (2019) 974-980.

[3] A. Dewan, P. Mahanta, K.S. Raju, P.S. Kumar, Review of passive heat transfer augmentation techniques, Proceedings of the Institution of Mechanical Engineers, Part A: Journal of Power and Energy, 218(7) (2004) 509-527.

[4] S. Liu, M. Sakr, A comprehensive review on passive heat transfer enhancements in pipe exchangers, Renewable and sustainable energy reviews, 19 (2013) 64-81.

[5] J. Zhao, S. Huang, L. Gong, Z. Huang, Numerical study and optimizing on micro square pin-fin heat sink for electronic cooling, Applied Thermal Engineering, 93 (2016) 1347-1359.

[6] S.-H. Park, T.H. Kim, J.H. Jeong, Experimental investigation of the convective heat transfer coefficient for open-cell porous metal fins at low Reynolds numbers, International Journal of Heat and Mass Transfer, 100 (2016) 608-614.

[7] J. Cheng, Z. Qian, Q. Wang, Analysis of heat transfer and flow resistance of twisted oval tube in low Reynolds number flow, International Journal of Heat and Mass Transfer, 109 (2017) 761-777.

[8] R.B. Bird, R.C. Armstrong, O. Hassager, C.F. Curtiss, Dynamics of polymeric liquids, Wiley New York, 1977.

[9] S.J. Muller, R.G. Larson, E.S.J.R.A. Shaqfeh, A purely elastic transition in Taylor-Couette flow, Rheol. Acta, 28(6) (1989) 499-503.

[10] R.G. Larson, E.S. Shaqfeh, S.J.J.J.o.F.M. Muller, A purely elastic instability in Taylor–Couette flow, J. Fluid Mech., 218 (1990) 573-600.

[11] A. Groisman, V.J.P.o.F. Steinberg, Mechanism of elastic instability in Couette flow of polymer solutions: experiment, Phys. Fluids, 10(10) (1998) 2451-2463.

[12] G. Vinogradov, V.J.K.-Z.u.Z.f.P. Manin, An experimental study of elastic turbulence, Kolloid Z. Z. Polym., 201(2) (1965) 93-98.

[13] Larson, Fluid dynamics: turbulence without inertia, Nature, 405(6782) (2000) 27.

[14] A. Groisman, V. Steinberg, Stretching of polymers in a random three-dimensional flow, Phys. Rev. Lett., 86(5) (2001) 934.

[15] A. Groisman, V. Steinberg, Elastic turbulence in a polymer solution flow, Nature, 405(6782) (2000) 53-55.

[16] B.A. Schiamberg, L.T. Shereda, H.U.A. Hu, R.G. Larson, Transitional pathway to elastic turbulence in torsional, parallel-plate flow of a polymer solution, J. Fluid Mech., 554(-1) (2006) 191.

[17] T. Burghelea, E. Segre, V. Steinberg, Elastic turbulence in von Karman swirling flow between two disks, Phys. Fluids, 19(5) (2007) 053104.

[18] A. Groisman, V. Steinberg, Elastic turbulence in curvilinear flows of polymer solutions, New Journal of Physics, 6(1) (2004) 29.

[19] N. Latrache, O. Crumeyrolle, I. Mutabazi, Transition to turbulence in a flow of a shear-thinning viscoelastic solution in a Taylor-Couette cell, Phys Rev E Stat Nonlin Soft Matter Phys, 86(5 Pt 2) (2012) 056305.

[20] J. Beaumont, N. Louvet, T. Divoux, M.-A. Fardin, H. Bodiguel, S. Lerouge, S. Manneville, A. Colin, Turbulent flows in highly elastic wormlike micelles, Soft Matter, 9(3) (2013) 735-749.

[21] T. Burghelea, E. Segre, I. Bar-Joseph, A. Groisman, V. Steinberg, Chaotic flow and efficient mixing in a microchannel with a polymer solution, Phys Rev E Stat Nonlin Soft Matter Phys, 69(6 Pt 2) (2004) 066305.

[22] Y. Jun, V. Steinberg, Elastic turbulence in a curvilinear channel flow, Phys Rev E Stat Nonlin Soft Matter Phys, 84(5 Pt 2) (2011) 056325.

[23] F.-C. Li, H. Kinoshita, X.-B. Li, M. Oishi, T. Fujii, M. Oshima, Creation of very-low-Reynolds-number chaotic fluid motions in microchannels using viscoelastic surfactant solution, Experimental Thermal and Fluid Science, 34(1) (2010) 20-27.
[24] H.Y. Gan, Y.C. Lam, N.-T. Nguyen, Polymer-based device for efficient mixing of viscoelastic fluids, Appl. Phys. Lett., 88(22) (2006) 224103.
[25] P.C. Sousa, F.T. Pinho, M.A. Alves, Purely-elastic flow instabilities and elastic turbulence in microfluidic cross-slot devices, Soft Matter, 14(8) (2018) 1344-1354.
[26] L. Pan, A. Morozov, C. Wagner, P.E. Arratia, Nonlinear elastic instability in channel flows at low Reynolds numbers, Phys. Rev. Lett., 110(17) (2013) 174502.
[27] B. Qin, P.E. Arratia, Characterizing elastic turbulence in channel flows at low Reynolds number, Physical Review Fluids, 2(8) (2017).
[28] A. Groisman, V. Steinberg, Efficient mixing at low Reynolds numbers using polymer additives, Nature, 410(6831) (2001) 905.
[29] T. Burghelea, E. Segre, V. Steinberg, Mixing by polymers: experimental test of decay regime of mixing, Phys. Rev. Lett., 92(16) (2004) 164501.
[30] H.Y. Gan, Y.C. Lam, N.T. Nguyen, K.C. Tam, C. Yang, Efficient mixing of viscoelastic fluids in a microchannel at low Reynolds number, Microfluidics and Nanofluidics, 3(1) (2006) 101-108.
[31] S. Li, H. Zhang, J. Cheng, X. Li, W. Cai, Z. Li, F. Li, A state-of-the-art overview on the developing trend of heat transfer enhancement by single-phase flow at micro scale, International Journal of Heat and Mass Transfer, 143 (2019) 118476.
[32] B. Traore, C. Castelain, T. Burghelea, Efficient heat transfer in a regime of elastic turbulence, Journal of Non-Newtonian Fluid Mechanics, 223 (2015) 62-76.
[33] R. Whalley, W. Abed, D. Dennis, R. Poole, Enhancing heat transfer at the micro-scale using elastic turbulence, Theoretical and Applied Mechanics Letters, 5(3) (2015) 103-106.
[34] W.M. Abed, R.D. Whalley, D.J.C. Dennis, R.J. Poole, Experimental investigation of the impact of elastic turbulence on heat transfer in a serpentine channel, Journal of Non-Newtonian Fluid Mechanics, 231 (2016) 68-78.
[35] D.-Y. Li, X.-B. Li, H.-N. Zhang, F.-C. Li, S.-Z. Qian, S.W. Joo, Measuring heat transfer performance of viscoelastic fluid flow in curved microchannel using Ti–Pt film temperature sensor, Experimental Thermal and Fluid Science, 77 (2016) 226-233.
[36] D.-Y. Li, X.-B. Li, H.-N. Zhang, F.-C. Li, S. Qian, S.W. Joo, Efficient heat transfer enhancement by elastic turbulence with polymer solution in a curved microchannel, Microfluidics and Nanofluidics, 21(1) (2017).
[37] D. Copeland, C. Ren, M. Su, P. Ligrani, Elastic turbulence influences and convective heat transfer within a miniature viscous disk pump, International Journal of Heat and Mass Transfer, 108 (2017) 1764-1774.
[38] P. Ligrani, D. Copeland, C. Ren, M. Su, M. Suzuki, Heat Transfer Enhancements from Elastic Turbulence Using Sucrose-Based Polymer Solutions, Journal of Thermophysics and Heat Transfer, 32(1) (2017) 51-60.
[39] Ç. Şahin, K. Atalık, Effects of polymer/surfactant additives on forced convective heat transfer in vortex shedding flow past a circular cylinder, International Journal of Thermal Sciences, 145 (2019) 106031.
[40] P.M. Ligrani, M. Su, A. Pippert, R.A. Handler, Thermal Transport of Viscoelastic Fluids Within Rotating Couette Flows, Journal of Thermophysics and Heat Transfer, 34(1) (2020) 121-133.
[41] A. Minaeian, M. Nili-Ahmadabadi, M. Norouzi, Forced convective heat transfer of nonlinear viscoelastic flows over a circular cylinder at low Reynolds inertia regime, Communications in Nonlinear Science and Numerical Simulation, 83 (2020) 105134.
[42] K. Tatsumi, W. Nagasaka, R. Kimura, N. Shinotsuka, R. Kuriyama, K. Nakabe, Local flow and heat transfer characteristics of viscoelastic fluid in a serpentine channel, International Journal of Heat and Mass Transfer, 138 (2019) 432-442.
[43] H. Yang, G. Yao, D. Wen, Experimental investigation on convective heat transfer of Shear-thinning fluids by elastic turbulence in a serpentine channel, Experimental Thermal and Fluid Science, 112 (2020) 109997.

[44] P. Li, Y. Xie, D. Zhang, Laminar flow and forced convective heat transfer of shear-thinning power-law fluids in dimpled and protruded microchannels, International Journal of Heat and Mass Transfer, 99 (2016) 372-382.
[45] C. Scholz, F. Wirner, J.R. Gomez-Solano, C. Bechinger, Enhanced dispersion by elastic turbulence in porous media, EPL (Europhysics Letters), 107(5) (2014) 54003.
[46] A. Clarke, A.M. Howe, J. Mitchell, J. Staniland, L. Hawkes, K. Leeper, Mechanism of anomalously increased oil displacement with aqueous viscoelastic polymer solutions, Soft Matter, 11(18) (2015) 3536-3541.
[47] A.M. Howe, A. Clarke, D. Giernalczyk, Flow of concentrated viscoelastic polymer solutions in porous media: effect of M(W) and concentration on elastic turbulence onset in various geometries, Soft Matter, 11(32) (2015) 6419-6431.
[48] G. Yao, J. Zhao, S.B. Ramisetti, D. Wen, Atomistic Molecular Dynamic Simulation of Dilute Poly(acrylic acid) Solution: Effects of Simulation Size Sensitivity and Ionic Strength, Industrial & Engineering Chemistry Research, 57(50) (2018) 17129-17141.
[49] R. Schweins, J. Hollmann, K. Huber, Dilute solution behaviour of sodium polyacrylate chains in aqueous NaCl solutions, Polymer, 44(23) (2003) 7131-7141.
[50] W.M. Abed, R.D. Whalley, D.J. Dennis, R.J. Poole, Numerical and experimental investigation of heat transfer and fluid flow characteristics in a micro-scale serpentine channel, International Journal of Heat and Mass Transfer, 88 (2015) 790-802.
[51] Y. Liu, Y. Jun, V. Steinberg, Longest relaxation times of double-stranded and single-stranded DNA, Macromolecules, 40(6) (2007) 2172-2176.
[52] Y. Jun, V. Steinberg, Polymer concentration and properties of elastic turbulence in a von Karman swirling flow, Physical Review Fluids, 2(10) (2017).
[53] J.P. Gollub, J. Clarke, M. Gharib, B. Lane, O. Mesquita, Fluctuations and transport in a stirred fluid with a mean gradient, Phys. Rev. Lett., 67(25) (1991) 3507.
[54] G. Yao, J. Zhao, H. Yang, M.A. Haruna, D. Wen, Effects of salinity on the onset of elastic turbulence in swirling flow and curvilinear microchannels, Phys. Fluids, 31(12) (2019) 123106.
[55] L. Casanellas, M.A. Alves, R.J. Poole, S. Lerouge, A. Lindner, The stabilizing effect of shear thinning on the onset of purely elastic instabilities in serpentine microflows, Soft Matter, 12(29) (2016) 6167-6175.
[56] A. Varshney, V. Steinberg, Drag enhancement and drag reduction in viscoelastic flow, Physical Review Fluids, 3(10) (2018) 103302.